Improved Electronic Properties with New Half-Metallic Ferromagnetic Behavior of $ZnCrO_2$ and $ZnMnO_2$ from TB-mBJ Exchange Potential

M. Tabti[a], B. Doumi[b,c], A. Mokaddem[b], A. Boudali[a,*], M.D. Khodja[a], A. Bentayeb[a] and H. Moujri[d]

[a]Laboratory of Physico-Chemical Studies, University of Saida, 20000 Saida, Algeria
[b]Laboratoire d'Instrumentation et Matériaux Avancés, Centre Universitaire Nour Bachir El-Bayadh, BP 900 route Aflou, 32000, Algeria
[c]Physics Department, Faculty of Science, University Dr. Tahar Moulay of Saida, Algeria
[d]Renewable Energy Laboratory and dynamic systems, Faculté des Sciences Ain-Chock, Université Hassan II de Casablanca, Morocco

(Received February 26, 2019; revised version August 30, 2019; in final form September 13, 2019)

We have performed a study of the structural, elastic, electronic, and magnetic properties of $ZnCrO_2$ and $ZnMnO_2$ chalcopyrite, using the Full-potential linearized augmented wave method (FP-LAPW), as part of the density functional theory (DFT). We have treated the exchange and correlation energy with the generalized gradient approximation (GGA-PBEsol) and the Tran-Blaha modified Becke-Johnson (TB-mBJ) meta-GGA. We have obtained new predictions for elastic properties. We have shown that these compounds are half-metals, and a spin polarization of 100% at the Fermi level. From these new results, we have predicted that these compounds are suitable in spintronic and optoelectronic applications.

DOI: 10.12693/APhysPolA.136.889

PACS/topics: GGA-PBEsol, TB-mBJ, half-metals, chalcopyrites, spintronic, optoelectronic

1. Introduction

The half-metal ferromagnets (HMF) are considered as materials that behave a metal in a one spin state and as a semiconductor in the opposite direction, and they show a complete spin polarization of 100% around the Fermi level (E_F). These compounds have experienced strong growth in various fields of application, in particular in spintronics as spin injection devices [1]. The Half-metallicity (HM) in the NiMnSb Heusler half-alloy was discovered by De Groot et al. [2]. According to this discovery, many HMF-based materials have been theoretically predicted and experimentally synthesized, for example, the zinc-blende compounds, organic hybrid compounds, pure organic compounds, and transition metal oxides [2, 3]. The chalcopyrites have been explored for practical applications in spintronics devices, because of their high Curie temperature and anti-ferromagnetism behavior and due their structural similarity with respect to conventional semiconductors.

The chalcopyrite compounds crystallize in a chalcopyrite structure centered at the tetragonal body. This structure is described by two external lattice parameters a and c, and by an internal parameter u, which is related to the displacement of the anion in the x direction. The chalcopyrite crystals show tetragonal distortion, where the ratio $c/a = 2$. Moreover, the anion generally adopts an equilibrium position by being closer to a pair of cations than the other. This, deformed tetrahedral coordination can be characterized by the internal parameter u, which corresponds to 1/4th of the ideal structure in a mixture of zinc [4]. In this work, we have studied the structural, electronic, and magnetic properties of the $ZnTMO_2$ (M = Cr and Mn) compounds using the density functional theory.

2. Computational details

Our study aims to calculate the structural properties such as lattice parameters, bulk modulus, and its derivative, the elastic, electronic, and magnetic properties of the $ZnCrO_2$ and $ZnMnO_2$ chalcopyrite by the ab-initio methods. The calculations were performed by using the linear potential augmented linear wave with full potential (FP-LAPW) implemented in the WIEN2k code [5] within density functional theory (DFT) [6], where the exchange and correlation energy is treated by the generalized gradient approximation (GGA-PBEsol) [7]. This exchange and correlation potential gives good results for the structural parameters compared to the local density approximation (LDA) [8] and the generalized gradient approximation of Perdew-Burke-Ernzerhof (GGA-PBE) [9]. For calculating the electronic and magnetic properties, we have used the GGA-PBEsol, GGA-PBEsol+U,

*corresponding author; e-mail: abdelkader.boudali54@gmail.com

and the Tran-Blaha modified Becke–Johnson TB–mBJ potential for comparison purposes [10, 11] Becke and Johnson (BJ) have proposed new formula for exchange potential related to atoms [10]. Tran and Blaha (TB) [11] have proposed modified version of this functional noted TB-mBJ, which is appropriate also for solids and surprisingly improved the band gap of the materials. It is better for calculating electronic structures with respect to the most commonly used calculation methods such as LDA or GGA [10–13].

The results are obtained with a convergence of the order of 10^{-4} Ry. We used for the sampling of the Brillouin zone a grid ($10 \times 10 \times 10$) with 56 special k-points. The muffin-tin radii (R_{MT}) of the constituent elements of the studied materials are 2.04, 1.81, 1.87, and 1.56 for Zn, Cr, Mn, and O, respectively. The cutoff energy is chosen equal to -6.0 Ry. The relativistic effects are taken into account by the use of the scalar relativistic approximation when calculating the electronic states.

3. Results and discussions

3.1. Structural proprieties

The Fig. 1 shows the optimizations of energies as a function of external lattice parameters a and c, and an internal parameter u for $ZnCrO_2$ and $ZnMnO_2$ compounds. We have calculated the structural parameters by using the Murnaghan equation given by the following expression [15]:

$$E(V) = E_0 + B_0 V_0 + \frac{V}{B_0' V_0} - \frac{1}{B_0' - 1} + \frac{\left(\frac{V_0}{V}\right)^{B_0'-1}}{B_0'(B_0' - 1)}$$

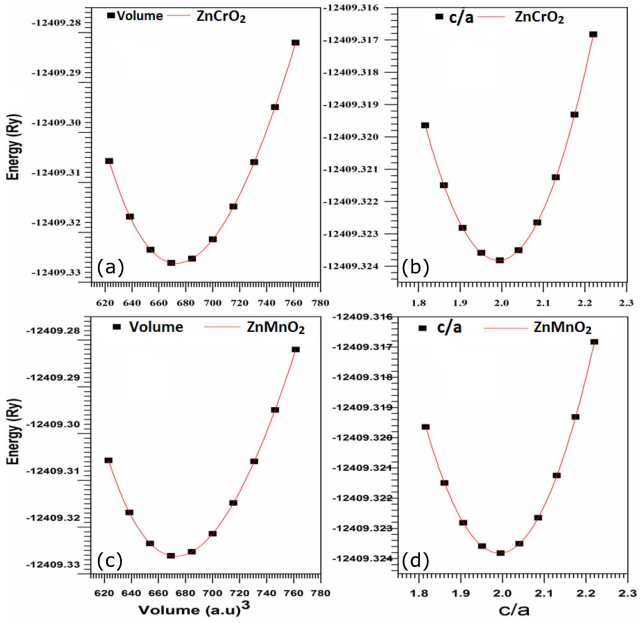

Fig. 1. Optimizations of energies as a function of volumes and c/a for $ZnCrO_2$ and $ZnMnO_2$.

TABLE I

Calculated equilibrium lattice parameters (a, b, c, c/a and u), bulk modulus (B) and its derivative (B') for $ZnCrO_2$ and $ZnMnO_2$ compounds.

Comp.	a [Å]	b [Å]	c [Å]	c/a	u	B [GPa]	B'
$ZnCrO_2$	4.70 4.71[a]	4.70 4.71[a]	9.40 9.42[a]	2.00 1.99[a]	0.245 0.245[a]	124.64 124.63[a] 125[b]	4.67 5.33[a]
$ZnMnO_2$	4.65 4.67[a]	4.65 4.67[a]	9.26 9.34[a]	1.99 2.00[a]	0.251 0.248[a] 141[b]	142.38 121.67[a]	4.60 5.85[a]

[a] Ref.[16], [b] Ref.[17]

The equilibrium value of c/a is calculated by fitting the polynomial equation of four degree that describes the total energies as a function of c/a. Our calculations are reported in Table I. The calculation of the adjustment parameter u is obtained through the minimization of the positions. Our results are in good agreement with the theoretical calculations [16, 17].

3.2. Elastic properties

The mechanical stability of a crystalline structure is originated from the formulation of M. Born and K. Huang [18]. The calculated elastic constants C_{ij} of the $ZnCrO_2$ and $ZnMnO_2$ compounds are presented in Table II. It can be seen that these constants are positive ($C_{11} > 0$, $C_{12} > 0$, $C_{13} > 0$, $C_{33} > 0$, $C_{66} > 0$, $C_{44} > 0$) and obey to Born's mechanical stability criterion for the tetragonal structures [19], i.e.,

$$C_{11} - C_{12} > 0, \quad C_{11} + C_{33} - 2C_{13} > 0$$

$$2\left(C_{11} + C_{12}\right) + C_{33} + 4C_{13} > 0$$

The compressibility module bulk modulus B is insufficient to fully describe the mechanical strength of a material. This value is related only to the normal pressing forces applied to its surface and does not take into account the tangential forces. It is necessary to introduce the shear modulus G related to the shear stresses given to the forces that act to move parallel plans of the solid in the direction of the force,

$$G = \frac{\tau_{xy}}{\gamma_{xy}} = \frac{Fl}{\Delta x A}.$$

The shear modulus G of the material is a better indicator of hardness than the bulk modulus.

There are three approximations for calculating the bulk modulus B and the shear modulus G for a single-phase structure. The first is the Voigt approximation [20], which determines the upper part of these parameters by using the elastic constants C_{ij} according to the following equations

$$B_{\mathrm{V}} = \frac{1}{9}\left(2C_{11} + 2C_{12} + C_{33} + 4C_{13}\right),$$

$$G_{\mathrm{V}} = \frac{1}{15}\left(2C_{11} - C_{12} + C_{33} - 2C_{13} + 6C_{44} + 3C_{66}\right).$$

TABLE II

The elastic parameters of $ZnCrO_2$ and $ZnMnO_2$ compounds.

Compound	C_{11}	C_{33}	C_{44}	C_{66}	C_{12}	C_{13}
$ZnCrO_2$	143.2	127.8	35.2	40.4	125.5	112.9
$ZnMnO_2$	163.8	149.5	39.6	40.9	134.7	135.3

The second is the Reuss method [21], which gives the lower limits of these parameters by using the flexibility coefficients S_{ij} [22, 23] according to the formulas below

$$B_{\mathrm{R}} = (2S_{11} + 2S_{12} + S_{33} + 4S_{13})^{-1},$$

$$G_{\mathrm{R}} = 15(8S_{11} - 4S_{12} + 4S_{33} - 8S_{13} + 6S_{44} + 3S_{66})^{-1}.$$

Based on Hill approximation [22], these two elastic modules represent the extreme limits (respectively a maximum for G_{V} and a minimum for G_{R}) of the real values of the polycrystalline constants. The actual value can be approximated through the arithmetic means of the following expressions

$$B_{\mathrm{H}} = \frac{B_{\mathrm{V}} + B_{\mathrm{R}}}{2}, \quad G_{\mathrm{H}} = \frac{G_{\mathrm{V}} + G_{\mathrm{R}}}{2}.$$

Finally, the Young's modulus E and the Poisson's ratio are calculated from the mean magnitudes as follows

$$E = \frac{9B_{\mathrm{H}}G_{\mathrm{H}}}{G_{\mathrm{H}} + 3B_{\mathrm{H}}}, \quad \upsilon = \frac{3B_{\mathrm{H}} - 2G_{\mathrm{H}}}{2(G_{\mathrm{H}} + 3B_{\mathrm{H}})}.$$

It is noteworthy that B measurement of incompressibility gives the resistance to the change of volume while G is a reliable indicator of hardness [23, 24]. Table III gives the elastic constants of bulk modulus B, shear modulus G, Young modulus E, Poisson's ratio, and anisotropy for $ZnCrO_2$ and $ZnMnO_2$ compounds.

To measure the ductility of materials, we use the Pugh ratio [24], which is a dimensionless quantity defined as $\mathrm{Pu} = B_{\mathrm{H}}/G_{\mathrm{H}}$.

The values found in our case (5.55 and 5.86) and are equally higher than the critical value. This indicates that the studied compounds ($ZnCrO_2$ and $ZnMnO_2$) are fragile, although having a ductile character. Our results of modulus B of chalcopyrites are very similar to those one, obtained with other studies, i.e., $B = 124.63$ GPa for $ZnCrO_2$ [16], and $B = 142.39$ GPa for $ZnMnO_2$ [17]. The shear modulus G, in turn, shows that the bonds between the atoms are stronger in $ZnCrO_2$ than $ZnMnO_2$. It is therefore necessary to apply intense shear forces to cause breaks in the chemical bonds between the atoms in these compounds. Thus, it is clear that the shear modulus G is a more significant hardness factor than the compressibility modulus B. The Young's modulus E of a material is the tension-strain ratio. It characterizes its stiffness. Physically the higher E is the more rigid the material is, the weaker E is the softer the material is. Table III shows that the Young's modulus values of our compounds are of the order of 73.84 and 51.22 GPa, which remain overall lower than that of the metals. This proves that our compounds have a more rigid behavior than metals.

Another fundamental concept of the mechanical properties of a crystal is elastic anisotropy, which explains the anisotropic nature of chemical bonds in different directions. To study the elastic anisotropy of $ZnCrO_2$ and $ZnMnO_2$, we adopted three approaches

1. The Voigt [20] model which describes the elastic anisotropy related to compressibility, is given by the formula
$$A_{\mathrm{G}} = \frac{G_{\mathrm{V}} - G_{\mathrm{R}}}{G_{\mathrm{V}} + G_{\mathrm{R}}},$$
2. The Reuss model [21] that characterize elastic anisotropy, is expressed by the following relation
$$A_{\mathrm{B}} = \frac{B_{\mathrm{V}} - B_{\mathrm{R}}}{B_{\mathrm{V}} + B_{\mathrm{R}}}.$$

These two coefficients are between the value 0, which indicates that the material is isotropic and the value 1 which shows that the compound has a maximum anisotropy.

Calculations for our solids show that the value A_{B} (0.97%) is much smaller than A_{G} (19%). This means that the compound has acquired more pronounced shear anisotropy than the compressibility anisotropy.

3 The third relation for anisotropy is a combination of G_{V}, G_{R}, B_{V} and B_{R}. It has a general aspect and is evaluated by the so-called universal anisotropy index [25, 26]:
$$AU = 5\frac{G_{\mathrm{V}}}{G_{\mathrm{R}}} + \frac{B_{\mathrm{V}}}{B_{\mathrm{V}}} - 6.$$

TABLE III

The other elastic parameters of ZnCrO2 and ZnMnO2 compounds.

Parameter	$ZnCrO_2$			$ZnMnO_2$		
	Voigt	Reuss	Hill	Voigt	Reuss	Hill
bulk modulus	124.1	121.7	122.9	143.1	142.3	142.7
shear modulus (Lame Mu)	26.3	17.9	22.1	28.83035	19.9	24.3
Lame lambda	106.5	109.8	108.1	123.91206	129.1	126.5
Young modulus	73.8	51.2	62	81.04927	57.1	69.2
Poisson ratio	0.40087	0.4	0.4	0.40562	0.4	0.4
universal anisotropy index		2.3			2.3	
elastic Debye temperature [K]		301.8			313.8	
averaged sound velocity [m/s]		2349.9			2426.4	

The value characterizes an isotropic character of the crystals whereas the deviations to the null value determine the anisotropic extension [27]. The calculated values of the test compounds are $AU = 2.37614$ and $AU = 2.37614$ for $ZnCrO_2$ and $ZnMnO_2$, respectively, showing appreciable elastic anisotropy.

3.3. The Electronic proprieties

3.3.1. Band structures

The discovery of semi-metallicity has developed several materials for spintronic applications of the magnetic tunnel junction [27–30], such as Sr_2FeMoO_6 [29–31], $La_{0.7}Sr_{0.3}MnO_3$ [31, 32], and the Co_2MnSi [32]. For the magnetic tunnel junction, in the anti-parallel configuration, the electrons do not cross the insulating barrier and the resistance is infinite. However, in the parallel configuration the electrons cross the barrier by the tunnel effect and the resistance is finite.

The calculated band structures of $ZnCrO_2$ and $ZnMnO_2$ with TB-mBJ potential are displayed in Figs. 2 and 3, respectively. In these plots one can see that the valence and the conduction band overlap, below Fermi level for majority-spin bands. This means then that the compounds have a metallic character. In turn,

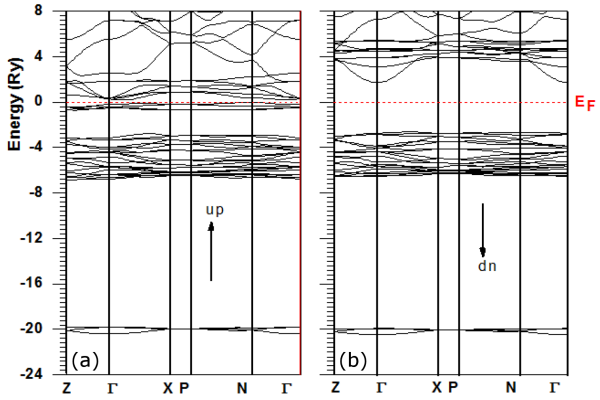

Fig. 2. Band structures of $ZnCrO_2$ with TB-mBJ potential. (a) Spin up, and (b) Spin down.

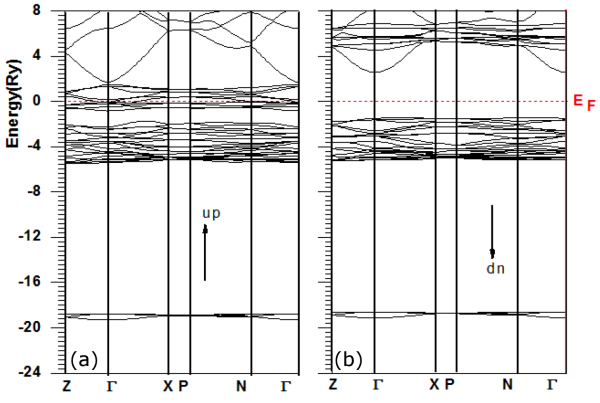

Fig. 3. Band structures of $ZnMnO_2$ with TB-mBJ potential. (a) Spin up and (b) Spin down.

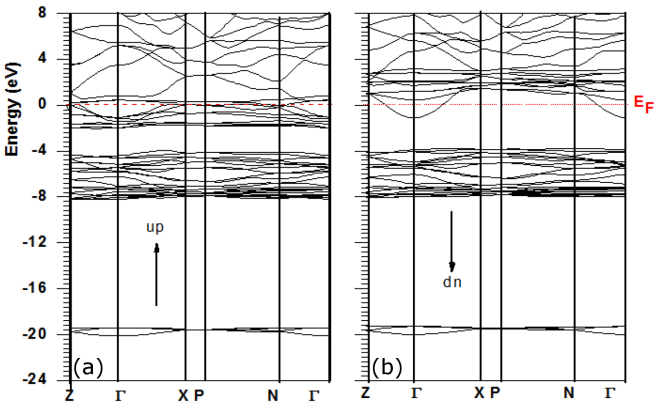

Fig. 4. Band structures of $ZnCrO_2$ with GGA-PBEsol potential. (a) Spin up and (b) Spin down.

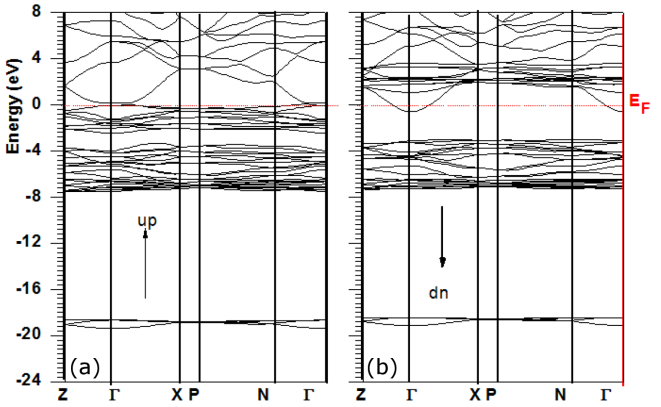

Fig. 5. Band structures of $ZnMnO_2$ with GGA-PBEsol potential. (a) Spin up, and (b) Spin down.

the minority-spin bands are semiconductors, because the band gaps occur between the valence and the conduction bands for both $ZnCrO_2$ and $ZnMnO_2$ compounds. Thus, we have deduced that our compounds are half-metals. In Figs. 4–7, the results of bands structures obtained by the GGA-PBEsol and GGA-PBEsol+U approximations show metallic character of the $ZnCrO_2$ and $ZnMnO_2$ compounds. According to [10, 11, 31–35], the LDA+U approach systematically improves the LDA band gap by acting indirectly on both the valence band maximum (VBM) and the minimum conduction band (CBM). In our case, the use of GGA-PBEsol+U improves the band structures. It moves VBM to downward and CBM to the top with respect to the Fermi level compared to the GGA-PBEsol. However the minority-spin bands of two compounds still remain metallic. In contrast, the TB-mBJ potential improves significantly the band structures. Then, the CBM is moved towards the higher energies above Fermi level, and hence the minority-spin bands of the two materials become semiconductor. Therefore, the $ZnCrO_2$ and $ZnMnO_2$ compounds show a half-metallic ferromagnetic behavior by the use of TB-mBJ exchange potential.

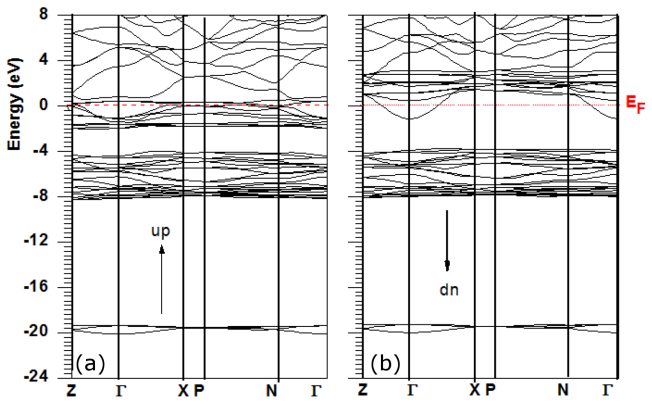

Fig. 6. Band structures of $ZnCrO_2$ with GGA-PBEsol+U potential. (a) Spin up, and (b) Spin down.

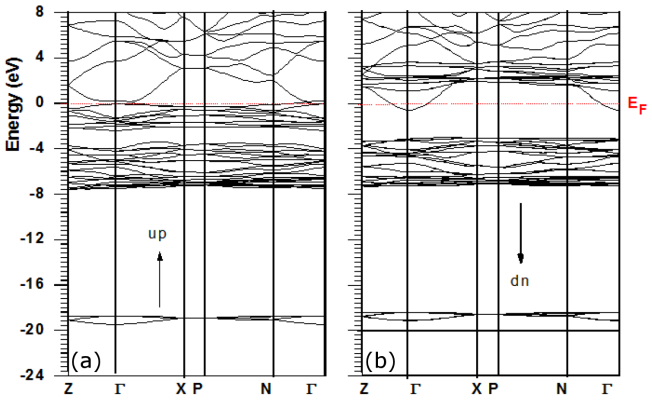

Fig. 7. Band structures of $ZnMnO_2$ with GGA-PBEsol+U potential. (a) Spin up, and (b) Spin down.

3.3.2. The Density of states

The density of states is generally used to comprehensively understand the electronic structure of a compound. Taking into account the spin polarization (spins up and down), the total density of states (TDOS) and the partial states densities (PDOS) of the $ZnCrO_2$ and $ZnMnO_2$ chalcopyrites in the ferromagnetic phase are calculated in its equilibrium state by GGA-PBEsol, GGA-PBEsol+U, and TB-mBJ [10, 31–35]. The densities of states (DOS) calculated by TB-mBJ are illustrated by Figs. 8 and 9. For the majority-spins states, the energy regions between 0 and −8.3 eV for $ZnCrO_2$ and between 0.17 and −7.1 eV for $ZnMnO_2$ are mainly originated by the contributions of the DOS of Cr 3*d* and O 2*p*, and Mn 3*d* and O 2*p* states. The second region of the B_V of sub-band of the semi-core, consists of the O-*s* states, which are localized between −19.96 and −20.64 eV for $ZnMnO_2$, and −21.07 and −21.93 eV and $ZnCrO_2$, respectively. The conduction bands between 0 and 10 eV, and 0.11 - 10 eV, are originated from Cr 3*d* and Mn 3*d* states for $ZnCrO_2$ and $ZnMnO_2$, respectively. For the minority-spin states, the total and partial densities of states have two bands and the valence band (V_B) have two sub-bands.

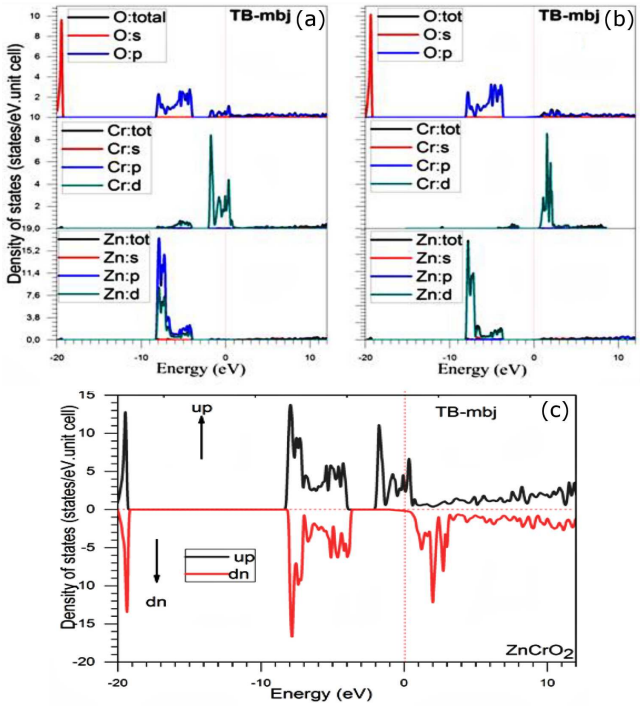

Fig. 8. Spin-polarized total and partial densities of states of $ZnCrO_2$ with TB-mBJ.

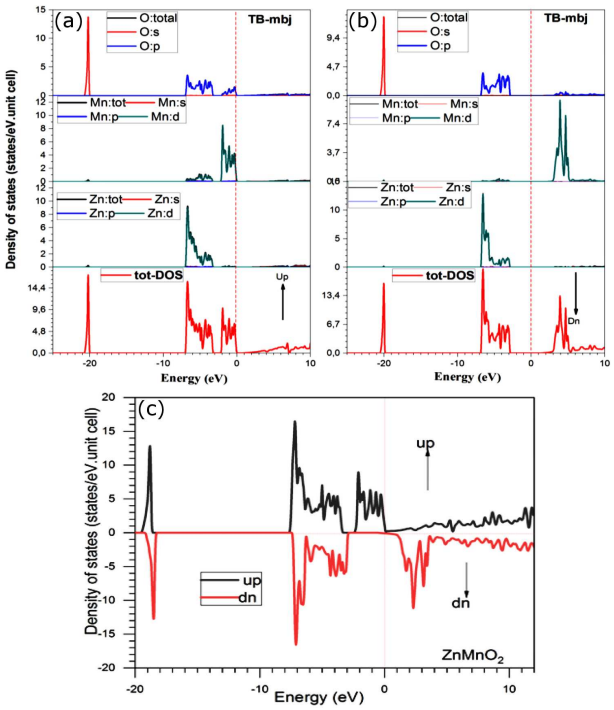

Fig. 9. Spin-polarized total and partial densities of states of $ZnMnO_2$ with TB-mBJ.

The top of the V_B between 0.11 and −8 eV for $ZnCrO_2$, and between −2.79352 and −6.9965 eV for $ZnMnO_2$, is due to Zn 3*d*, Zn 3*d*, and Mn 3*d* states. The bottom

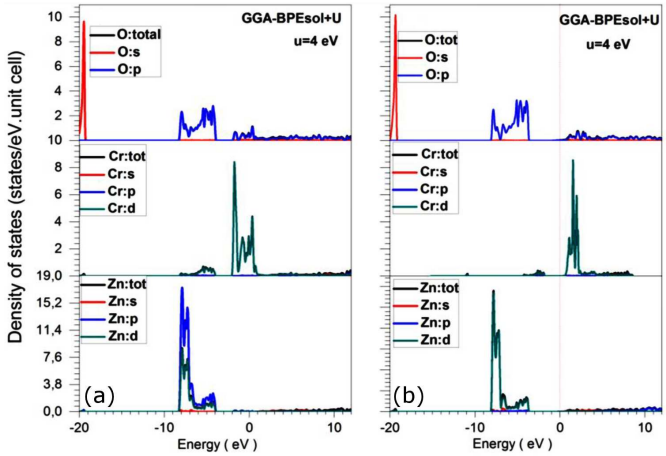

Fig. 10. Spin-polarized total and partial densities of states of $ZnCrO_2$ with GGA-PBEsol+U.

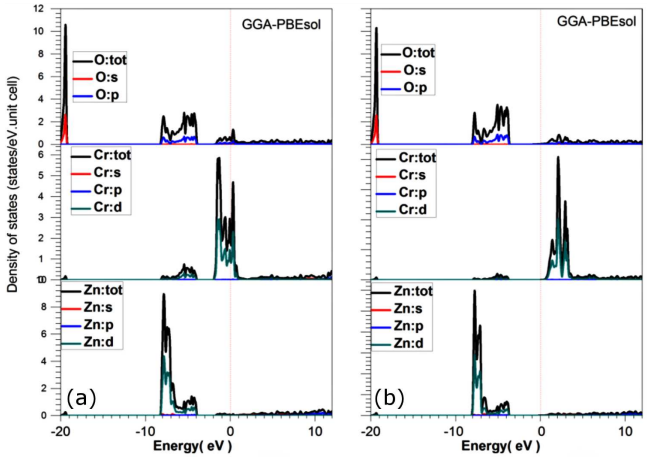

Fig. 12. Spin-polarized total and partial densities of states of $ZnCrO_2$ with GGA-PBEsol.

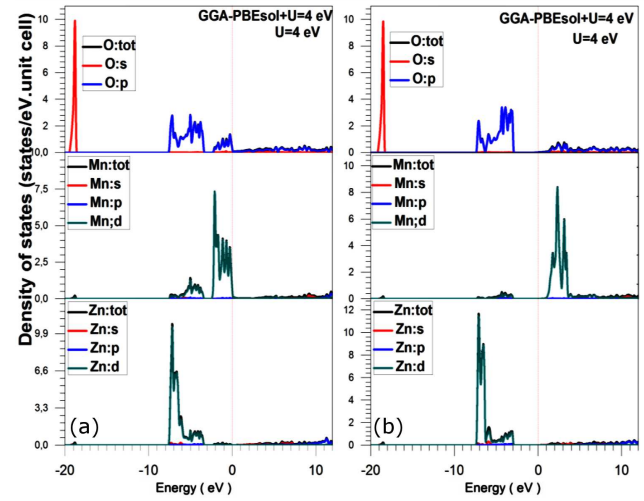

Fig. 11. Spin-polarized total and partial densities of states of $ZnMnO_2$ with GGA-PBEsol+U.

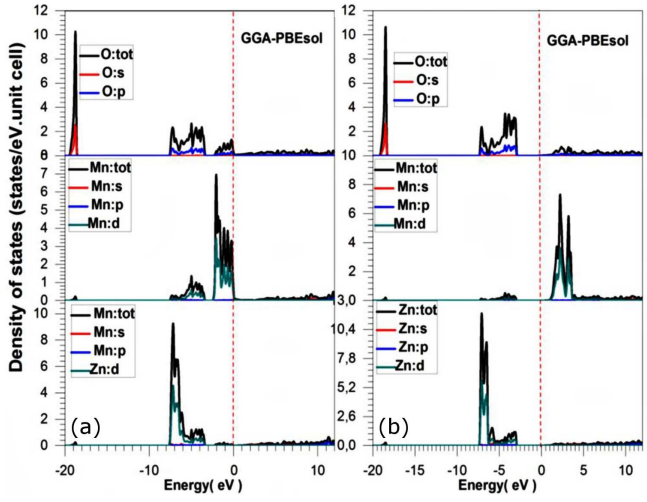

Fig. 13. Spin-polarized total and partial densities of states of $ZnMnO_2$ with GGA-PBEsol.

of semi-core states in the range −21.06 and −21.93 eV for $ZnCrO_2$, and in the range −19.96 and −20.81 eV for $ZnMnO_2$, are due to the O 2*s* states. The conduction bands in the range 0.11 and 10 eV for $ZnCrO_2$, and 1.23 and 10 eV for $ZnMnO_2$, are dominated by single bands, which are characterized by the Cr 3*d* and Mn 3*d* states. Therefore, the majority spins have a metallic character, and the minority spins have a gap of 4 and 4.03 eV for $ZnCrO_2$ and $ZnMnO_2$, respectively. From these findings, we have deduced that the $ZnCrO_2$ and $ZnMnO_2$ are half metals with spin polarizations about 100%.

We have performed GGA-PBEsol+U calculations with several values of U Hubbard ranging from 2 to 7 eV because the value U is not easy to estimate [30–35]. The obtained bands structures with different values of U have the same behavior. Figures 10–13 show the densities of states obtained with the GGA-PBEsol and GGA-PBEsol+U for $U = 4$ eV. For both $ZnCrO_2$ and $ZnMnO_2$ compounds, the majority and minority-spin states with GGA-PBEsol and GGA-PBEsol+U revealed overlaps between the valence and conduction bands. For the spin down channel, the valence and conduction bands are separated by a pseudo gap when using the GGA-PBEsol+U approximation [10, 35]. The densities minority-spin states calculated using the TB-mBJ potential have a gap that is not observed with the GGA-PBEsol+U. No difference is observed between the calculations obtained with the GGA-PBEsol+U and GGA-PBEsol. The band overlap at the Fermi level is due to the *p*–*d* hybridization between the O 2*p* and Cr 3*d* or Mn 3*d* states.

The observations that can be made comparing the results obtained with the TB-mBJ and the GGA-PBEsol+U are the following:

1. The GGA-PBEsol+U acts on both the valence and conduction bands: there is a split of bands and the gap becomes larger;

2. The TB-mBJ acts only on the conduction band, which decreases the width of conduction band and induces an increase in the gap. In the case of our calculations, this effect is observed only for the spin down channel.

3.4. The magnetic properties

The total magnetic moments of $ZnCrO_2$ and $ZnMnO_2$ compounds are the sum of the local magnetic moments of Zn, Cr, Mn, O atoms and the interstitial magnetic moment. The calculated magnetic moments by the TB-mBJ potential are summarized in Table IV. The obtained total magnetic moments are 8 μ_B and 10 μ_B for $ZnCrO_2$ and $ZnMnO_2$, respectively, which obey to the Hund's rule. The integral values of total magnetic moments indicate that these materials are true half-metallic ferromagnets. The values of total magnetic moments are formed by the main contributions of Cr and Mn transition elements, and small contributions occur at Zn and O sites and in the interstitial region with respect to the high total magnetic moments of compounds under study.

TABLE IV

The total and partial magnetic moments (in μ_B) of the $ZnCrO_2$ and $ZnMnO_2$ compounds.

Magnetic moment	$ZnCRO_2$	$ZnMnO_2$
in interstitial	1.61743	0.91720
in sphere Zn	0.02464	0.01783
in sphere Cr	3.20925	–
in sphere Mn	–	4.33686
in sphere O	−0.02079	0.09418
in cell $ZnCrO_2$	8.00204	–
in cell $ZnMnO_2$	–	10.00330

4. Conclusion

We have performed a study of structural, elastic, electronic, and magnetic properties of $ZnCrO_2$ and $ZnMnO_2$ chalcopyrite using the linearized augmented plane waves method (FP-LAPW), within density functional theory (DFT). We have treated the exchange and correlation energy with the PBEsol, GGA-PBEsol+U, and TB-mBJ potentials. We have obtained new predictions for elastic properties. We have found that the $ZnCrO_2$ and $ZnMnO_2$ compounds are half-metallic ferromagnetic with total magnetic moments 8 μ_B for $ZnCrO_2$ and 10 μ_B for $ZnMnO_2$ and spin polarization of 100% around Fermi level. From these findings, the $ZnCrO_2$ and $ZnMnO_2$ chalcopyrites seem to be potential materials for spintronics field.

References

[1] H. Van Luken, R.A. de Groot, *Phys. Rev. Lett.* **74**, 1171 (1995).

[2] R.A. de Groot, F.M. Mueller, P.G. van Engen, K.H.J. Buschow, *Phys. Rev. Lett.* **50**, 2024 (1983).

[3] H.M. Huang. S.J. Luo, K.L. Yao, *J. Supercond. Nov. Magn.* **27**, 257 (2014).

[4] J.E. Jaffe, A. Zunger, *Phys. Rev. B* **29**, 1882 (1984).

[5] P. Blaha, K. Schwarz, G.K.H. Madsen, D. Kvasnicka, J. Luitz, in: *WIEN2K: An Augmented Plane Wave Plus Local Orbitals Program for Calculating Crystal Properties*, Ed. K. Schwarz, Vienna University of Technology, Austria (2001).

[6] W. Kohn, L.J. Sham, *Phys. Rev.* **140** , 1133 (1965).

[7] J.P. Perdew, A. Ruzsinszky, G.I. Csonka, O.A. Vydrov, G.E. Scuseria, L.A. Constantin, X. Zhou, K. Burke, *Phys. Rev. Lett.* **100**, 136406 (2008).

[8] J.P. Perdew, Y. Wang, *Phys. Rev. B.* **45**, 13244 (1992).

[9] J.P. Perdew, K. Burke, M. Ernzerhof, *Phys. Rev. Lett.* **77**, 3865 (1996).

[10] A.D. Becke, E.R. Johnson, *J. Chem. Phys.* **124**, 221101 (2006).

[11] F. Tran, P. Blaha, *Phys. Rev. Lett.* **102**, 226401 (2009).

[12] A. Koralewski, R. Armiento, S. Kümmel, *J. Chem. Theory Comput.* **5**, 712 (2009).

[13] A.P. Gaiduk, V.N. Staroverov, *J. Chem. Phys.* **131**, 044107 (2009).

[14] M. Shishkin, M. Marsman, G. Kresse, *Phys. Rev. Lett.* **99**, 246403 (2007).

[15] F.D. Murnaghan, *Proc. Natl. Acad. Sci.* **30**, 244 (1944).

[16] R. Merikhi, B. Bennecer, A. Hamidani, *J. Magn. Magn. Mater.* **15**, 327 (2017).

[17] R. Thangavel, M. Rajagopalan, J. Kumar, *J. Magn. Magn. Mater.* **320**, 774 (2008).

[18] U.F. Ozyar , E.Deligoz , K. Colakoglu, *Solid State Sci.* **40**, 92 (2015).

[19] M. Kalay, H. Kart, S.ʹO. Kart, T. Çagin, *J. Alloys Comp.* **484**, 431 (2009).

[20] W. Voigt, *Lehrbuch der Kristallpysik Taubner*, p. 29. Leipzig, 1928.

[21] A. Reuss, *J. Appl. Math. Mech.* **9**, 55 (1929).

[22] R. Hill, *Proc Phys. Soc.* **65**, 349 (1952).

[23] M.J. den Toonder, J.A.W. van Dommelen, F.P.T. Baaijens, *Modell. Simul. Mater. Sci. Eng.* **7**, 909 (1999).

[24] S.F. Pugh, *Philos. Mag.* **45**, 823 (1954).

[25] S.I. Ranganathan, M. Ostoja-Starzewski, *Phys. Rev. Lett.* **101**, 055504 (2008).

[26] C.T. Tanaka, J. Nowak, J.S. Moodera, *J. Appl. Phys.* **86**,6239 (1999).

[27] C.V. Tiusan, Ph.D. Thesis, Université Louis Pastereur de Strasbourg, 2000.

[28] M. Besse, Ph.D. Thesis, l'Unité Mixte de Recherche CNRS / Thales, 2003.

[29] E. Favre-Nicolin, Ph.D. Thesis, Université de Grenoble I — Joseph Fourier, 2003.

[30] N.D. Telling, P.S. Keatley, G. van der Laan, R.J. Hicken, E. Arenholz, Y. Sakuraba, M. Oogane, Y. Ando, T. Miyazaki, *Phys. Rev. B.* **74**, 224439 (2006).

[31] L. Wu, T. Hou, Y. Wang, Y. Zhao, Z. Guo, Y. Li , S.T. Lee, *J. Alloys Compd.* **541**, 250 (2012).

[32] J. Kaczkowski, A. Jezierski, *Acta Phys. Pol. A* **116**, 924 (2009).

[33] D. Iuşan, B. Sanyal, O. Eriksson, *Phys. Rev. B*, **74**, 235208 (2006).

[34] J. Kaczkowski, M.P. Michalska, A. Jezierski, *Acta Phys. Pol. A* **127**, 266 (2015).

[35] A. Janotti, D. Segev, C.G. Van de Walle, *Phys. Rev. B* **74**, 045202 (2006).